symmetry

MDPI

Article

Unsteady Electro-Hydrodynamic Stagnating Point Flow of Hybridized Nanofluid via a Convectively Heated Enlarging (Dwindling) Surface with Velocity Slippage and Heat Generation

Abbas Khan [1], Wasim Jamshed [2,*], Mohamed R. Eid [3,4], Amjad Ali Pasha [5], El Sayed M. Tag El Din [6], Hamiden Abd El-Wahed Khalifa [7,8] and Samaher Khalaf Alharbi [9]

1 Department of Mathematics, University of Haripur, Haripur 22620, Pakistan
2 Department of Mathematics, Capital University of Science and Technology (CUST), Islamabad 44000, Pakistan
3 Department of Mathematics, Faculty of Science, New Valley University, Al-Kharga 72511, Egypt
4 Department of Mathematics, Faculty of Science, Northern Border University, Arar 1321, Saudi Arabia
5 Aerospace Engineering Department, King Abdulaziz University, Jeddah 21589, Saudi Arabia
6 Electrical Engineering, Faculty of Engineering and Technology, Future University in Egypt, New Cairo 11835, Egypt
7 Department of Operations Research, Faculty of Graduate Studies for Statistical Research, Cairo University, Giza 13613, Egypt
8 Department of Mathematics, College of Science and Arts, Qassim University, Al-Badaya 51951, Saudi Arabia
9 Department of Mathematics, College of Science and Arts, Qassim University, Ar Rass 51921, Saudi Arabia
* Correspondence: wasiktk@hotmail.com

Abstract: In (Al_2O_3-Cu/H_2O) hybridized nanofluid (HYNF) is an unsteady electro-hydrodynamic stagnation point flow. A stretchable (shrinkable) surface that was convectively heated was studied in the past. In addition to the traditional nonslip surface, the heat generating (absorbing) and the velocity slippage constraints are deliberated in this research. An obtained nonlinear scheme is resolved by the homotopy analysis method. Governing parameters are the electric field parameters, that is, the dimensionless parameters including the magnetic parameter, Prandtl quantity, heat generating factor, Eckert quantity, and unsteady factor. We discuss in detail the effects of these variables on the movement of problems and thermal transmission characteristics. Increasing the values of the magneto and electric force parameters increased the temperature. Increasing the Prandtl number lowered the temperature. For the Eckert parameter, an increase in temperature was recognized. The symmetric form of the geometry model displayed improved the fluid flow by the same amount both above and below the stagnation streamline, while it decreased the flow pressure by the same level. The more heat source uses to increase the temperature of the HYNF over the entire area, the more heat is supplied to the plate, but with a heat sink, the opposite effect is observed.

Keywords: hybridized nanofluid; unsteadiness stagnating point; velocity slippage; convective boundary constraint; magnetic nanofluid; electric field; homotopy analysis method (HAM)

check for updates

Citation: Khan, A.; Jamshed, W.; Eid, M.R.; Pasha, A.A.; Tag El Din, E.S.M.; Khalifa, H.A.E.-W.; Alharbi, S.K. Unsteady Electro-Hydrodynamic Stagnating Point Flow of Hybridized Nanofluid via a Convectively Heated Enlarging (Dwindling) Surface with Velocity Slippage and Heat Generation. *Symmetry* **2022**, *14*, 2136. https://doi.org/10.3390/sym14102136

Academic Editors: Sergei D. Odintsov and Ghulam Rasool

Received: 9 September 2022
Accepted: 10 October 2022
Published: 13 October 2022

1. Introduction

Nanofluids have gained increasing attention due to their ability to recover heat transfer efficiency in an assortment of industrial presentations, as well as the considerable upsurge in the thermal conducting of the subsequent liquid. As a continuation of nanofluids, HYNFs can be made by diffusing compound nano-powders or numerous types of nanomolecules in the solution. HYNF is an innovative nanoliquid with two separate nanoparticles immersed in the base fluid.

In recent years, many scholars have been involved in researching the heat transfer of HYNF because HYNFs exhibit a higher heat transfer coefficient than conventional nanofluids. As a result, most heat transfer applications (e.g., machined coolants and HYNF) have been explored to increase the thermal transmission coefficient of traditional nanoliquids.

Several authors used computational techniques to observe the boundary layer flow and thermal transmission of HYNFs. For example, Devi and Devi [1] used Cu-Al_2O_3 magnetically effective nanoparticles to revise the flow of HYNFs through elastic surfaces. This problem was then extended by Devi [2] to a three-dimensional flow that follows Newton's heating conditions. They exposed that the heat transmission factor of HYNFs was greater than that of regular nanofluids in both studies. Hayat and Nadeem [3] considered the issue of (Ag-CuO/water) and HYNF that does not shake concerning rotating currents. The consequence of rapid slippage on heat transmission in an unsteady stagnating point flow of HYNF throughout a convective-heated enlarging (dwindling) plate was examined by Zainal et al. [4]. Daniel et al. [5] investigated unstable combined natural and forced convective electrical magnetohydrodynamic (MHD) flow and thermal transmission across a transparent stretched layer using the Buongiorno model. Xie et al. [6] investigated the frictional force factor and put it on a quantity of hybridized nanomolecules to evaluate their tribological assets. HYNFs have reduced wear and coefficient of friction compared to pure nanofluids, according to Devi et al. [2] examination on three-dimensional flow of (Cu-Al_2O_3/H_2O) HYNF using the RK Fehlberg integration process. Considering the Lorentz force, the movement is caused by the unidirectional linear elongation of a flat surface. Numerical results suggest that the heat exchange ratio of (Cu-Al_2O_3) HYNF is more advanced than that of the mono nanoliquid. The impact of temperature distribution and nanoparticle attention on the rheological interest of a magnetite ferrofluid silver/ethylene glycol (Fe_3O_4-Ag/EG) HYNF was studied by Afrand et al. [7].

In the existence of Lorentz forces, Ghadikolaei et al. [8] explored the physical and thermal characteristics of (TiO_2-Cu/H_2O) HYNF with shape factor. Hussian et al. [9] investigated the flow of HYNF covering (Cu-Al_2O_3/H_2O) combination via an open hollow space with an adiabatic square obstruction in the hollow space. They calculated numerical answers to the usage of the finite detail technique and explored the effect of numerous physical parameters on HYNFs.

Magnetohydrodynamics (MHD) has recently gained attention due to its extensive selection of solicitations in engineering, chemical knowledge, petroleum use, the environment, and geophysics. MHD implements a magneto force, usually orthogonal to the flow of liquid, which can generate the Lorentz force, which is a drag. This force faces the flow of the fluid and affects the velocity of the fluid, which tends to be critical [10]. We found that power-law fluid MHD combined convective flows over a nonlinearly stretched layer. Zhao et al. reported on the impact of magneto heat transmission regarding nanoliquids in micro-channels [11]. Many more major works in this field are attributed to refs. [12–14].

Scientists are interested in strained surfaces for a variety of engineering applications such as blown glass, cooling of microelectronics, metal foundry quenching, wire drawing, polymer extrusion, and high-speed spraying. The theoretical boundary layer flow on an expanding surface was discovered by Crane [15]. Exponentially expanding surface area [16–19] and important industrial and technological applications have been studied by many researchers. In everyday life and industry, exponentially contracting/expanding surfaces are frequently used for liquid flow and thermal transfer. A study by Magyari and Keller [20] seems to have initially addressed the flow of the fluid boundary layer on an exponential expanding plate. The exponential comparison variable was calculated by Mushtaq et al. [21] to convert the predominant PDE to ODE. In addition, Reddy et al. [22] studied the mixed convection of nanofluids on an exponential surface and observed that the concentricity, momentum, and thickness of the thermal boundary layer increased as the viscosity ratio parameter increased. The stagnating point MHD flow model was developed by Rahman et al. [23], who generated the ODE using the exponential similarity variable.

The liquid movement at the rigid surface's stagnating point is represented by the stagnating point flow. Hiemenz1 [24] was the main researcher to probe the problem of fluid stagnating points flowing via a rigid surface. Homann [25] extended these concerns to the case of axis symmetry for the flow of 3D stagnation spots. Meanwhile, he reported a stream of stagnation towards the contracting plate. In the work of Wang [26], the presence of stagnant flow rates could limit turbulence and maintain flow, excluding the need to apply suction to the shrinking film. Several researchers have extended the stagnation point flow problem to the effects of different flow behaviors. For example, the problem is present with or without heat transfer melting, studied by Bachok et al. [27]. They did not find a solution.

The heat transfer coefficient at the solid–liquid boundary tends to decrease only when shrinking and when increasing the melting parameters. Fang and Wang [28] also studied the flow of temporary stagnation points to the movable plate and provided an accurate result to the problem. In the fields of mathematics, fluid mechanics, and engineering, several approximation methods have been used to solve real problems. In 1992, Liao [29] learned that this method was a quick fix and better suited for solving nonlinear problems. Homotopy analysis (HAM) [30–32] was used for the solution.

This study aims to investigate the interactions between an electrical force, a magnetic field, a magneto force, and heat-producing (absorbing) impacts in a conductive HYNF that integrates stability analysis and rapid slippage parameters. The incorporation of hybrid nanoparticles aids in the stabilizing of a nanofluid's motion and retains the symmetry of the moving configuration. Due to the above problems, researchers are now encouraged to perform numerical studies with unstable stagnation point flow on alumina–copper–water convection heating plates (alumina, copper-to-water) under the influence of a reduced heat transfer coefficient. Using the appropriate set of dimensionless variables to reduce the independent variables of the mathematical model equations, the analytical solution was calculated using the homotopy method.

2. Mathematical Formulation

In this research work, as illustrated in Figure 1, the unsteady 2D stagnation point flow of (Al_2O_3-Cu/H_2O) HYNF above a convective-heated stretchable (shrinkable) plate influencing the speed of slippage is deliberated.

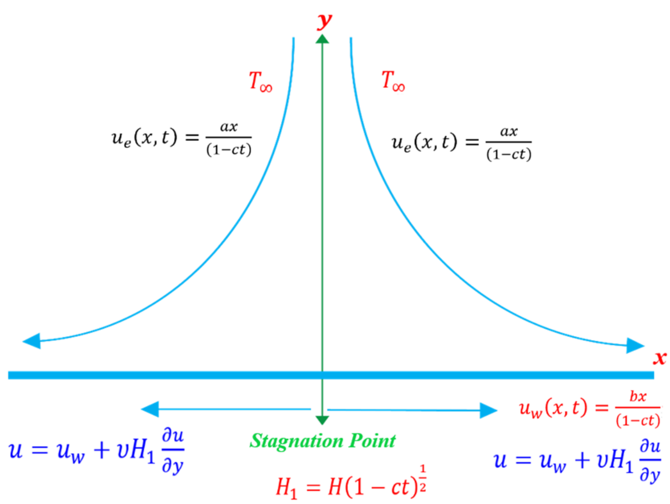

Figure 1. Flow model scheme diagram.

The extending/shrinking velocity is marked by $u_w(x,t) = \frac{bx}{(1-ct)}$, where b represents constant stretchable ($b > 0$) and a shrinkable ($b < 0$) cases, while c indicates the time-based issue, $a > 0$ signifies the asset of the flow of stagnations, and $u_e(x,t) = \frac{ax}{(1-ct)}$ is the speed of the free stream. T_1 and T_0 stand for the free temperature and the standard temperature, respectively. We let the bottom of the surface warm up by convective heat from a hot liquid at a certain temperature $T_f(x,t) = T_1 - T_0 \frac{ax^2}{2v}(1-ct)^{-\frac{3}{2}}$, which generated a heat transfer coefficient, denoted by h_f. Taking into account all of the aforementioned hypotheses, the regulating boundary layer formulas may be identified as [4]:

$$\frac{\partial u}{\partial x}+\frac{\partial u}{\partial y}=0, \tag{1}$$

$$\frac{\partial u}{\partial t}+u\frac{\partial u}{\partial x}+v\frac{\partial u}{\partial y}=\frac{\partial u_e}{\partial t}+u_e\frac{\partial u_e}{\partial x}+\frac{\mu_{hnf}}{\rho_{hnf}}\frac{\partial^2 u}{\partial y^2}+\frac{\sigma_{hnf}}{\rho_{hnf}}\left(E_0B_0-B_0^2u\right), \tag{2}$$

$$\frac{\partial T}{\partial t}+u\frac{\partial T}{\partial x}+v\frac{\partial T}{\partial y}=\frac{k_{hnf}}{(\rho c_p)_{hnf}}\frac{\partial^2 T}{\partial y^2}+\frac{\sigma_{hnf}}{(\rho c_p)_{hnf}}(B_0u-E_0)^2+\frac{Q_0}{(\rho c_p)_{hnf}}(T-T_\infty), \tag{3}$$

where v is the velocity factor in y-axis, u symbolizes the elements of rapidity in x-axis, μ_{hnf} is the (Al_2O_3-Cu/H_2O) dynamic viscosity, ρ_{hnf} the consistency of (Al_2O_3-Cu/H_2O), T is the HYNF temperature, $(\rho c_p)_{hnf}$ is HYNF heat capacity, and k_{hnf} is the thermal conductance. The boundary conditions, composed through the restricted slippage for rapidity, are established as:

$$\left.\begin{array}{l} u=u_w(x,t)+vH_1\frac{\partial u}{\partial y}, v=0, -k_{hnf}\frac{\partial T}{\partial y}=h_f\left(T_f-T\right)\ at\ y=0, \\ u\to u_e(x,t), T\to T_\infty\ as\ y\to\infty. \end{array}\right\} \tag{4}$$

where $H_1=H(1-ct)^{\frac{1}{2}}$ is the quickness slippage variable, and H denotes the original value of the speed slippage variable. Copper (Cu) physical–thermal characteristics, laterally with aluminum-oxide (Al_2O_3) and H_2O nanomolecules, are provided in Table 1. Table 2 shows the physical–thermal characteristics of HYNF. The nanomolecules' volumetric fraction is denoted by ϕ, ρ_f specifies H_2O consistency, ρ_s is the consistency of the nanosolid particles, c_p is the continuous pressure of heat capacity, k_f symbolizes the thermal conductivity of H_2O, and k_s is the nanoparticles' thermal conductivity.

Table 1. Cu thermophysical properties laterally with Al_2O_3 and H_2O [4].

Properties	Cu	Al_2O_3	H_2O
$k(W/mK)$	400	40	0.613
$\rho\left(kg/m^3\right)$	8933	3970	9971
$c_p(J/kgK)$	385	765	4179
$\beta\times10^5\left(\frac{1}{K}\right)$	1.67	0.85	21

Table 2. Utilized relations for physical–thermal characteristics of HYNF [4].

Characteristic	HYNF
μ	$\mu_{hnf}=\frac{1}{\left(1-\phi_{hnf}\right)^{2.5}}$
ρ	$\rho_{hnf}=\left(1-\phi_{hnf}\right)\rho_f+\phi_1\rho_{s1}+\phi_2\rho_{s2}$
(ρc_p)	$(\rho c_p)_{hnf}=\left(1-\phi_{hnf}\right)(\rho c_p)_f+\phi_1(\rho c_p)_{s1}+\phi_2(\rho c_p)_{s2}$
k	$\frac{k_{hnf}}{k_f}=\left[\frac{\left(\frac{\phi_1k_{s1}+\phi_2k_{s2}}{\phi_{hnf}}\right)+2k_f+2(\phi_1k_{s1}+\phi_2k_{s2})-2\phi_{hnf}k_f}{\left(\frac{\phi_1k_{s1}+\phi_2k_{s2}}{\phi_{hnf}}\right)+2k_f-2(\phi_1k_{s1}+\phi_2k_{s2})+\phi_{hnf}k_f}\right]$

The following similarity transformations are presented [4] in the context of the governing Equations (1)–(3) about boundary conditions (4).

$$\psi=\left(\frac{av}{1-ct}\right)^{\frac{1}{2}}xf(\eta), \theta(\eta)=\frac{T-T_\infty}{T_f-T_\infty}, \eta=\left[\frac{a}{v(1-ct)}\right]^{\frac{1}{2}}y, \tag{5}$$

Here, ψ is the streaming function which is obtained from relations $u = \frac{\partial\psi}{\partial y}, v = -\frac{\partial\psi}{\partial x}$, and η is a similar variant. Consequently, we achieve

$$u = \frac{ax}{1-ct} f'(\eta), v = -\left(\frac{av}{1-ct}\right)^{\frac{1}{2}} f(\eta). \tag{6}$$

Concerning these relations, Equations (2) and (3) diminish the difference between the subsequent sets of nonlinear similitudes by using the similarity variables (5) and (6).

$$\frac{\frac{\mu_{hnf}}{\mu_f}}{\frac{\rho_{hnf}}{\rho_f}} f''' + ff'' - f'^2 + 1 - \varepsilon\left(f' + \frac{1}{2}\eta f'' - 1\right) + \frac{\frac{\sigma_{hnf}}{\sigma_f}}{\frac{\rho_{hnf}}{\rho_f}} M\left(E - f'\right) = 0, \tag{7}$$

$$\frac{1}{Pr} \frac{\frac{k_{hnf}}{k_f}}{\frac{(\rho c_p)_{hnf}}{(\rho c_p)_f}} \theta'' + f\theta' - 2f'\theta + \frac{\varepsilon}{2}\left(\eta\theta' + 3\theta\right) + \frac{\frac{\sigma_{hnf}}{\sigma_f}}{\frac{(\rho c_p)_{hnf}}{\rho_f}} MEc\left(f' - E\right) + \frac{Q(\rho c_p)_f}{(\rho c_p)_{hnf}} \theta = 0. \tag{8}$$

Then, the initial and limit conditions (4) are transformed in

$$\left.\begin{array}{l} f(0) = 0, f'(0) = \lambda + \gamma f''(0), -\frac{k_{hnf}}{k_f}\theta'(0) = Bi[1 - \theta(0)], \\ f'(\infty) \to 1, \theta(\infty) \to 0, \end{array}\right\} \tag{9}$$

In the following, $\varepsilon, M, E, Ec, Pr, Bi, Re_x, \lambda$, and Q are time-dependent parameter, magneto force, electrical force parameters, Eckert, Prandtl, Biot, Reynolds numbers in x-axis, the proportion of speed slippage, and heat generating (absorbing) parameter:

$$\left.\begin{array}{c} \lambda = \frac{b}{a}, \varepsilon = \frac{c}{a}, Re_x = \frac{u_e x}{\nu_f}, Pr = \frac{\nu_f}{\alpha}, M = \frac{\sigma\beta_0^2}{\rho_f a},\ \gamma = H\left(a\nu_f\right)^{\frac{1}{2}} \\ Bi = \frac{h_f}{k_f}\sqrt{\frac{\nu_f(1-ct)}{a}}, Ec = \frac{ax^2}{c_p \Delta T}, Q = \frac{Q_0(1-ct)^2}{ax}, E = \frac{E_0}{\beta_0 ax}. \end{array}\right\} \tag{10}$$

For the above model, the frictional surface force $\left(C_f\right)$ and Nusselt amount (Nu_x) remain clear as follows

$$C_f = \frac{\tau_w}{\rho_f u_e^2}, Nu_x = \frac{xq_w}{k_f\left(T_f - T_\infty\right)} \tag{11}$$

where

$$\tau_w = \mu_{hnf}\left(\frac{\partial u}{\partial y}\right)_{y=0}, q_w = -k_{hnf}\left(\frac{\partial T}{\partial y}\right)\Big|_{y=0}, \tag{12}$$

In the dimensional form, we have from above

$$Re_x^{1/2} C_f = \frac{\mu_{hnf}}{\mu_f} f''(0), Re_x^{-1/2} Nu_x = -\frac{k_{hnf}}{k_f}\theta'(0). \tag{13}$$

3. HAM Solution

The HAM is used to solve Equations (7) and (8) using the boundary condition (9). Mathematica software was used for this. In Figure 2, the HAM approach includes the following steps.

The model equations are described as fundamental derivations using HAM.

$$L_{\widehat{f}}\left(\widehat{f}\right) = \widehat{f}''', \ L_{\widehat{\theta}}\left(\widehat{\theta}\right) = \widehat{\theta}'' - \widehat{\theta} \tag{14}$$

Linear operators $L_{\widehat{f}}$, *and* $L_{\widehat{\theta}}$ are defined by

$$L_{\widehat{f}}\left(\gamma_1+\gamma_2 e^{-\eta}+\gamma_3 e^{\eta}\right)=0, L_{\widehat{\theta}}\left(\gamma_4 e^{-\eta}+\gamma_5 e^{\eta}\right)=0. \tag{15}$$

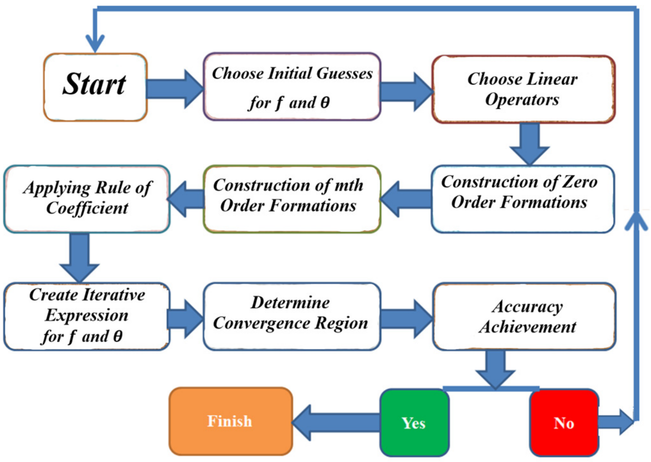

Figure 2. Flow chart.

The nonlinear operators are $N_{\widehat{f}}$ and $N_{\widehat{\theta}}$ that are identified in the structure:

$$N_{\widehat{f}}\left[\widehat{f}(\eta;\zeta)\right]=\frac{\frac{\mu_{hnf}}{\mu_f}}{\frac{\rho_{hnf}}{\rho_f}}\widehat{f}_{\eta\eta\eta}+\widehat{f}\widehat{f}_{\eta\eta}-\widehat{f}_{\eta}^{2}+1-\varepsilon\left(\widehat{f}_{\eta}+\frac{1}{2}\eta\widehat{f}_{\eta\eta}-1\right)+\frac{\frac{\sigma_{hnf}}{\sigma_f}}{\frac{\rho_{hnf}}{\rho_f}}M\left(E-\widehat{f}_{\eta}\right), \tag{16}$$

$$\begin{aligned}&N_{\widehat{\theta}}\left[\widehat{f}(\eta;\zeta),\widehat{\theta}(\eta;\zeta),\widehat{\phi}(\eta;\zeta)\right]\\&=\frac{1}{Pr}\frac{\frac{k_{hnf}}{k_f}}{\frac{(\rho c_p)_{hnf}}{(\rho c_p)_f}}\widehat{\theta}_{\eta\eta}+\widehat{f}\widehat{\theta}_{\eta}-2\widehat{f}_{\eta}\widehat{\theta}+\frac{\varepsilon}{2}(\eta\widehat{\theta}_{\eta}+3\widehat{\theta})+\frac{\frac{\sigma_{hnf}}{\sigma_f}}{\frac{(\rho c_p)_{hnf}}{\rho_f}}MEc(\widehat{f}_{\eta}-E)+\frac{Q(\rho c_p)_f}{(\rho c_p)_{hnf}}\theta\end{aligned} \tag{17}$$

For Equations (7) and (8) the 0th-order structure is exposed as

$$(1-\zeta)L_{\widehat{f}}\left[\widehat{f}(\eta;\zeta)-\widehat{f}_0(\eta)\right]=p\hbar_{\widehat{f}}N_{\widehat{f}}\left[\widehat{f}(\eta;\zeta)\right] \tag{18}$$

$$(1-\zeta)\,L_{\widehat{\theta}}\left[\widehat{\theta}(\eta;\zeta)-\widehat{\theta}_0(\eta)\right]=p\hbar_{\widehat{\theta}}N_{\widehat{\theta}}\left[\widehat{\theta}(\eta;\zeta),\widehat{f}(\eta;\zeta)\right] \tag{19}$$

Though BCs are

$$\left.\begin{array}{c}\widehat{f}(\eta;\zeta)\Big|_{\eta=0}=0,\ \frac{\partial\widehat{f}(\eta;\zeta)}{\partial\eta}\Big|_{\eta=0}=\lambda+\gamma\widehat{f}_{\eta\eta}(0),\ f(0)=0,\\ \frac{k_{nf}}{k_f}\frac{\partial\widehat{\theta}(\eta;\zeta)}{\partial\eta}\Big|_{\eta=0}=-Bi\left(1-\widehat{\theta}(0)\right),\ \frac{\partial\widehat{f}(\eta;\zeta)}{\partial\eta}\Big|_{\eta=\infty}\to 1,\ \widehat{\theta}(\eta;\zeta)\Big|_{\eta=\infty}\to 0,\end{array}\right\} \tag{20}$$

The embedding constraint is $\zeta\in[0,1]$, and to regulate the result converging $\hbar_{\widehat{f}}$ and $\hbar_{\widehat{\theta}}$ are utilized. At $\zeta=0$ and $\zeta=1$ we have:

$$\widehat{f}(\eta;1)=\widehat{f}(\eta),\widehat{\theta}(\eta;1)=\widehat{\theta}(\eta)\,, \tag{21}$$

Enlarging the $\widehat{f}(\eta;\zeta)$ and $\widehat{\theta}(\eta;\zeta)$ over Taylor's series for $\zeta = 0$, we obtain:

$$\left.\begin{array}{l}\widehat{f}(\eta;\zeta) = \widehat{f}_0(\eta) + \sum_{n=1}^{\infty} \widehat{f}_n(\eta)\zeta^n, \\ \widehat{\theta}(\eta;\zeta) = \widehat{\theta}_0(\eta) + \sum_{n=1}^{\infty} \widehat{\theta}_n(\eta)\zeta^n\end{array}\right\} \tag{22}$$

$$\widehat{f}_n(\eta) = \frac{1}{n!}\frac{\partial \widehat{f}(\eta;\zeta)}{\partial \eta}\Bigg|_{p=0}, \widehat{\theta}_n(\eta) = \frac{1}{n!}\frac{\partial \widehat{\theta}(\eta;\zeta)}{\partial \eta}\Bigg|_{p=0}, \tag{23}$$

BCs are:

$$\left.\begin{array}{l}\widehat{f}(0) = 0, \widehat{f}'(0) = \lambda + \gamma \widehat{f}''(0), -\frac{k_{hnf}}{k_f}\widehat{\theta}'(0) = Bi\left[1 - \widehat{\theta}(0)\right], \\ \widehat{f}'(\infty) \to 1, \widehat{\theta}(\infty) \to 0,\end{array}\right\} \tag{24}$$

Now,

$$\Re_n^{\widehat{f}}(\eta) = \frac{\frac{\mu_{hnf}}{\mu_f}}{\frac{\rho_{hnf}}{\rho_f}}\widehat{f}'''_{n-1} + \sum_{j=0}^{w-1}\widehat{f}_{w-1-j}f_j'' + 1 - \varepsilon\left(\widehat{f}'_{n-1} + \frac{1}{2}\eta \widehat{f}''_{n-1} - 1\right) + \frac{\frac{\sigma_{hnf}}{\sigma_f}}{\frac{\rho_{hnf}}{\rho_f}}M\left(E - \widehat{f}'_{n-1}\right) \tag{25}$$

$$\begin{array}{c}\Re_n^{\widehat{\theta}}(\eta) = \frac{1}{\Pr}\frac{\frac{k_{hnf}}{k_f}}{(\rho c_p)_{hnf}/(\rho c_p)_f}\left(\widehat{\theta}''_{n-1}\right) + \sum_{j=0}^{w-1}\widehat{\theta}'_{w-1-j}\hat{f}_j - 2\sum_{j=0}^{w-1}\widehat{\theta}_{w-1-j}\widehat{f}'_j + \frac{\varepsilon}{2}\left(\eta\widehat{\theta}'_{n-1} + 3\widehat{\theta}_{n-1}\right) + \\ \frac{\sigma_{hnf}/\sigma_f}{(\rho c_p)_{hnf}/\rho_f}MEc\left(\widehat{f}'_{n-1} - E\right) + \frac{Q(\rho c_p)_f}{(\rho c_p)_{hnf}}\widehat{\theta}_{n-1},\end{array} \tag{26}$$

where

$$\chi_n = \begin{cases} 0, \text{ if } n \leq 1 \\ 1, \text{ if } n > 1. \end{cases} \tag{27}$$

4. Results and Discussion

This study solved a homotopy analysis system for the transformed calculations of momentum, energy, and concentration ((7), (8)). Computational analysis was performed using various parameters such as Prandtl quantity, magneto force, electric field, time-dependent parameter, Eckert number, and parameter of heat source/sink. Figures 3–5 show various implanted parameters: electric field, magnetic field, and discontinuous velocity profile $f'(\eta)$.

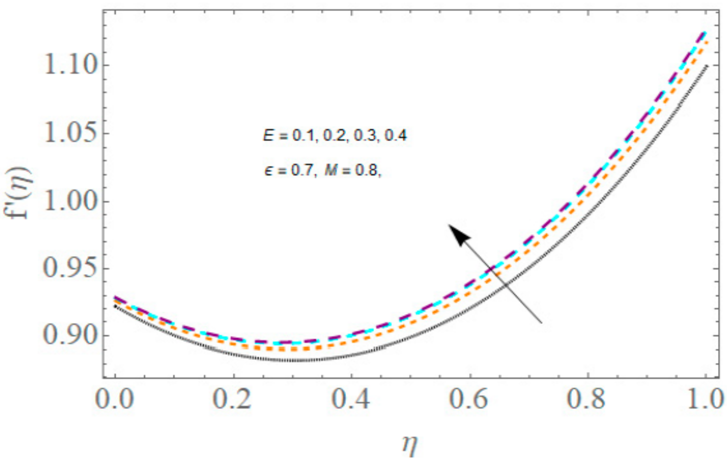

Figure 3. Effect of E on $f'(\eta)$.

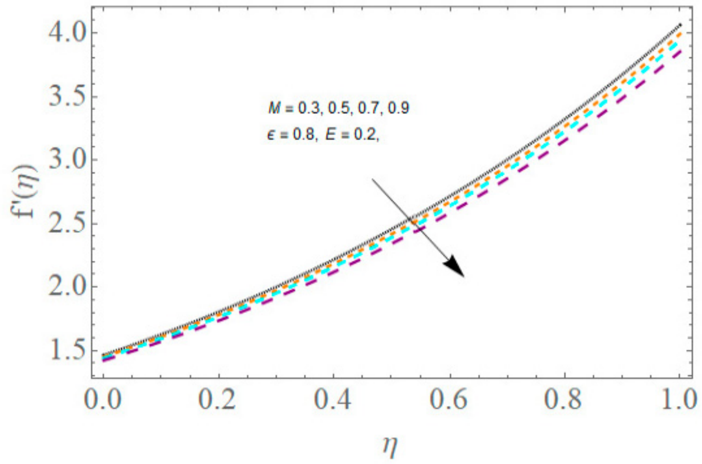

Figure 4. Effect of M on $f'(\eta)$.

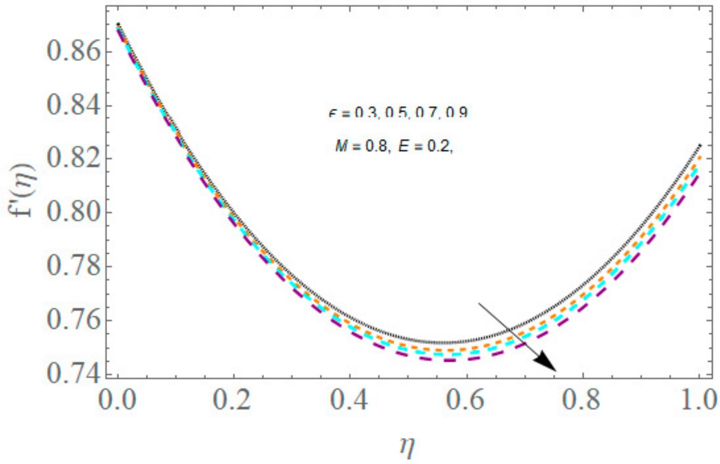

Figure 5. Consequence of ε on $f'(\eta)$.

Figure 3 specifies that as the electric parameter values rise, the rate of HYNF will increase. Electrical parameters act as accelerating forces. The better the Lorentz pressure and the smaller the Lorentz pressure, the better the electric confinement. A more potent Lorentz pressure will increase and release the stick impact with liquid nanoparticles that imply improved convection warmth switch and the width of the boundary momentum layer. The electric force increases the stored internal energy of the particles, which leads to an increase in the movement within the liquid, as a result of the increased collisions between the particles and each other and as a result of the internal acceleration among them. Figure 4 indicates the impact of the magneto force constraint M on the rate profile of HYNF. The better the magneto parameter value the more the width of the rate-momentum boundary layer is diminished. The magnetic area creates a drag referred to as the Lorenz wave that opposes the flow. This creates resistance to fluid flow, slows down, and decreases the width of the boundary layer. Thus, it works to slow the movement of particles within the fluid, which in turn reduces the general velocity of the fluid as a result of this increased resistance. Figure 5 indicates the impact of the unsteadiness parameter at the nanoliquid pace profile. This conduct is because of the deceleration case, which boosts the momentum boundary layer thickness and decreases HYNF flow. As the acceleration increases, the flow rate profile decreases. Over time, the internal energy of the molecules is lost, and thus the overall movement of the fluid is reduced.

In addition, Figures 6–11 show the properties of Eckert amount Ec, time-dependent variant ε, heat source/sink Q, magneto force constraint M, electrical force E, and Prandtl amount Pr on the temperature outlines $\theta(\eta)$. In Figure 6, when the kinetic energy to enthalpy ratio rises with a rise in the Ec, the temperatures of the nanoliquid increase, as does the width of the thermal boundary layer. This leads to an increase in heat dissipation within the HYNF. The effect of the unsteadiness parameter on $\theta(\eta)$ outlined in Figure 7 is contrary to the speed behavior in Figure 5. The unsteadiness parameter works overtime to make the molecules dissipate the stored energy internally, which boosts the heat transfer process, which in turn raises the temperature of the hybrid nanoliquid. It is obvious that the temperature is more affected by unsteadiness and increment values of it. The consequence of heat generation (absorption) on $\theta(\eta)$ is shown in Figures 8 and 9. It is shown that the heat source $(Q > 0)$ rises the fluid's temperature and the width of the temperature boundary layer, although the heat absorption $(Q < 0)$ delivers a diminution in $\theta(\eta)$ and slimmer temperature boundary layer width. $Q = 0$ implies the lack of heat generation (absorption). Figure 10 launches the effect of magneto force variant M on the nanoliquid energy contours. The width of the thermal boundary layer has risen owing to the transverse magnetic field. As a result, the thickness of the thermal boundary layer and $\theta(\eta)$ outlines are improved. The magneto force performs as a sturdy Lorentz power, growing $\theta(\eta)$ of the nanoliquid inside a border area. Lorentz forces work to boost the internally stored energy inside the nanomolecules, which leads to an excess in the temperature of the nanofluid and thus restores its movement, which reverses the effect between the rapidity of movement and the temperature as a result of raising the value of the magnetic field applied to the fluid. The influence of the electrical force variant at the temperature outline is found in Figure 11. The electric power performs as a speed-up force, boosting the nanoliquid temperature and developing the thickness of the temperature boundary layer. A wider, higher capacity $\theta(\eta)$ outline inside the boundary layer in proximity to the HYNF is hooked up with a larger amount of an electrical power variant. Higher Prandtl's quantities range is very satisfactory and differs from one fluid to the next. Figure 11 demonstrates that as it improves, the nanoliquid energy drops. The diffusivity impetus is more than the thermal diffusion for big values. As a result, the thickener of the energy boundary layer diminishes. The excess in the Prandtl quantity diminishes the thermal diffusivity factor as well as the boost in the viscidness of the hybrid nanoliquid, which in turn reduces the temperature of the hybrid nanoliquid as a whole, and this is the effect that is observed in the figure. In most warmness switch problems, the comparative thickness of each thermal boundary layer is reduced. Table 3 shows that C_f is enlarged after the standards of M, ε, E are enlarged. Table 4 displays that Nu_x is enlarged once the standards of M, Q are enlarged. Nu_x is diminished as the standards of Pr, E, Ec are enlarged.

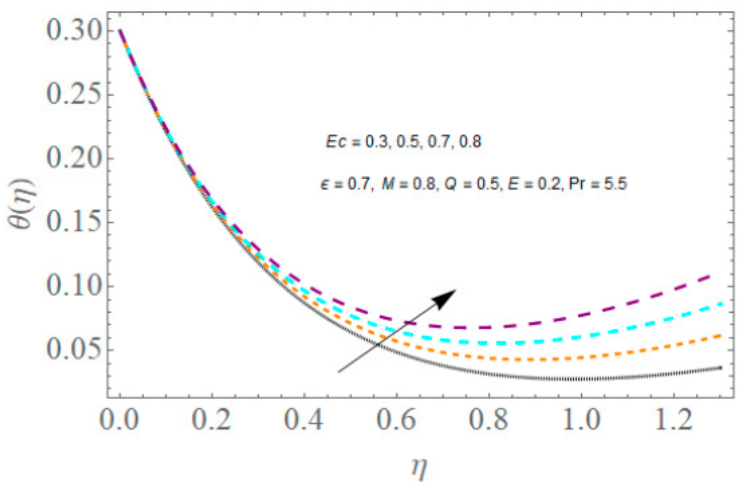

Figure 6. Consequence of Ec on $\theta(\eta)$.

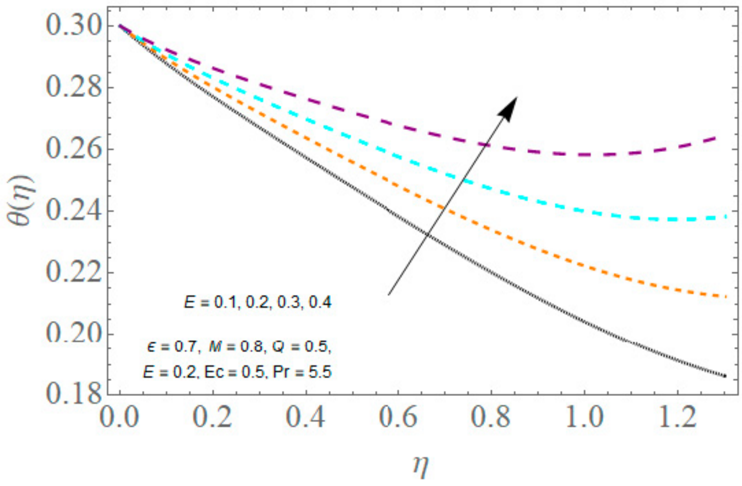

Figure 7. Consequence of ε on $\theta(\eta)$.

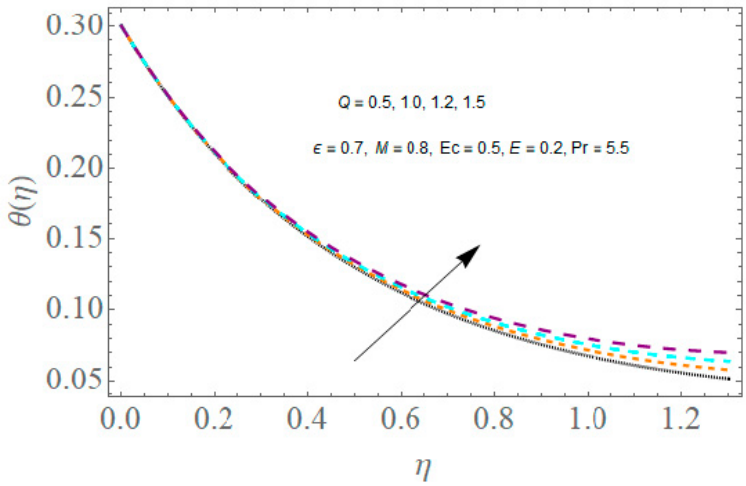

Figure 8. Consequence of $Q > 0$ on $\theta(\eta)$.

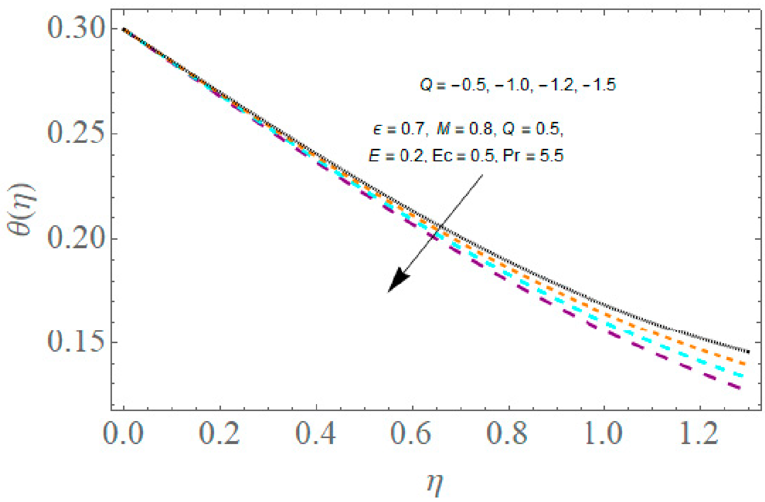

Figure 9. Consequence of $Q < 0$ on $\theta(\eta)$.

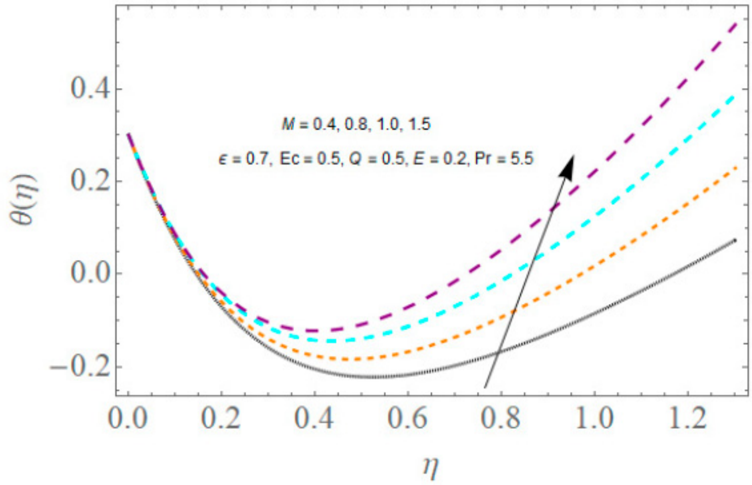

Figure 10. Consequence of M on $\theta(\eta)$.

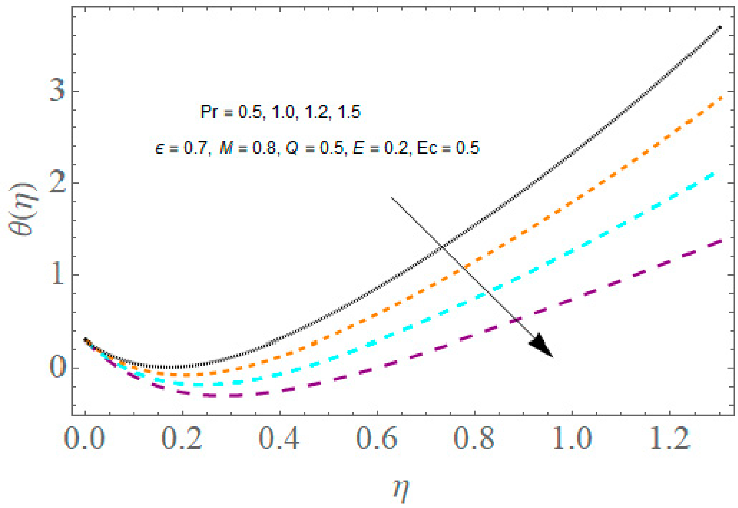

Figure 11. Effect of Pr on $\theta(\eta)$.

Table 3. Effect of various physical parameters on skin friction $Re_x^{1/2}C_f = \frac{\mu_{hnf}}{\mu_f} f''(0)$.

ε	E	M	$\frac{\mu_{hnf}}{\mu_f} f''(0)$
0.3	0.1	0.4	0.72059328
0.5			0.83542092
0.7			1.03614135
	0.1		1.86313569
	0.2		1.64385204
	0.3		1.76103193
		0.4	1.03873708
		0.8	1.30863981
		1.0	1.58376213

Table 4. Consequence of various physical parameters on Nusselt number $\left[-\frac{k_{hnf}}{k_f}\theta'(0)\right]$.

Ec	***Q***	***Pr***	***M***	***E***	$-\frac{k_{hnf}}{k_f}\theta'(0)$
0.3	0.5	4.5	0.4	0.1	1.07386504
0.5					1.17290347
0.7					1.23893104
	0.5				2.30319769
	1.0				2.15912307
	1.5				2.02463073
		4.5			0.54354079
		5.5			0.73865302
		6.5			0.93865321
			0.4		1.13159603
			0.8		1.09764384
			1.0		1.05346068
				0.1	1.12183304
				0.2	1.23583931
				0.3	1.30346893

5. Conclusions

An evaluation of the unstable electro-hydrodynamic stagnation factor float of HYNF via a convective heated stretchable (shrinkable) plate including the speed slippage effect on the heat switch is investigated in this study. Electrical and magneto forces and heat generating (absorbing) parameters were measured. The principal equations of the system were transmuted to nonlinear regular differential equalities with the use of similar variants and then resolved via the homotopy analysis method. The effects of numerous variables on pace and temperature were examined. Mathematical consequences of pace gradient and warmth switch quotes in opposition to numerous parameters were deliberated. The following are the most important observations of the study:

- Speed and temperature rise with a rise in an electrical constraint.
- Magnetic constraint has an inverted influence on rapidity and energy parameters.
- Heat generation increases the temperature, while the converse happens with a heat sink.
- Higher values of the unsteadiness constraint decrease the velocity and temperature.
- An augmentation in temperature is observed for Eckert amount, while it decreases for the Prandtl number.

The current technique could be implemented in other fields of science and engineering, especially when related to the simulation of fluid dynamics in the future [33–36].

Author Contributions: Conceptualization, A.K., W.J. and M.R.E.; methodology, A.K., W.J. and M.R.E.; software, A.K., W.J. and M.R.E.; validation, A.K., W.J. and M.R.E.; formal analysis, W.J., M.R.E. and S.K.A.; investigation, E.S.M.T.E.D., H.A.E.-W.K. and S.K.A.; resources, A.K., W.J. and M.R.E.; data curation, A.A.P.; writing—original draft preparation, W.J., M.R.E. and A.A.P.; writing—review and editing, A.K., W.J. and M.R.E.; visualization, E.S.M.T.E.D. and H.A.E.-W.K.; supervision, M.R.E.; project administration, W.J.; funding acquisition, S.K.A. All authors have read and agreed to the published version of the manuscript.

Funding: This research received no external funding.

Institutional Review Board Statement: Not applicable.

Informed Consent Statement: Not applicable.

Data Availability Statement: Not applicable.

Acknowledgments: The researchers would like to thank the Deanship of Scientific Research, Qassim University, for funding the publication of this project.

Conflicts of Interest: The authors declare no conflict of interest.

Nomenclature

u and v	quickness elements (m/s)
u_w	stretching/shrinking rapidity (m/s)
T_1	ambient temperature (K)
h_f	heat transmission factor
k_{hnf}	thermal conductance
μ_{hnf}	viscidness $\left(kgm^{-1}s^{-1}\right)$
Re_x	Reynolds quantity
H_1	quickness slippage factor
ρ_s	nanoparticle density $\left(kgm^{-3}\right)$
k_s	solid thermal conductance $\left(Wm^{-1}K^{-1}\right)$
ψ	stream function
M^*	magnetic parameter
Ec	Eckert Number
Bi	Biot amount
λ	rapidity and heat ratio
Nu_x	local Nusselt number
$f\prime$	non-dimensional rapidity
υ	kinematic viscidness $\left(m^2s^{-1}\right)$
ϕ	nanoparticle solid volume fraction
x,y	plane coordinate axis
u_e	strength of stagnation flow
T_0	reference temperature (K)
ρ_{hnf}	density $\left(kgm^{-3}\right)$
$\left(\rho c_p\right)_{hnf}$	volume heat capacitance $\left(m^2s^{-2}K^{-1}\right)$
η	similarity parameter
H	primary speed slippage
c_p	constant pressure of heat capacity
ρ_f	Base fluid density $\left(kgm^{-3}\right)$
k_f	fluid thermal conductance $\left(Wm^{-1}K^{-1}\right)$
ε	unsteady factor
E	electrical force factor
Pr	Prandtl number
Q	heat generating (absorbing)
c_f	skin friction factor
T	temperature of fluid (K)
μ_f	dynamical viscidness $\left(kgm^{-1}s^{-1}\right)$
τ_w	wall shear stress
q_w	transportation of heat

References

1. Devi, S.A.; Devi, S.S.U. Numerical investigation of hydromagnetic hybrid Cu–Al_2O_3/water nanofluid flow over a permeable stretching sheet with suction. *Int. J. Nonlinear Sci. Numer. Simul.* **2016**, *17*, 249–257. [CrossRef]
2. Devi, S.S.U.; Devi, S.A. Numerical investigation of three-dimensional hybrid Cu–Al_2O_3/water nanofluid flow over a stretching sheet with effecting Lorentz force subject to Newtonian heating. *Can. J. Phys.* **2016**, *94*, 490–496. [CrossRef]
3. Hayat, T.; Nadeem, S. Heat transfer enhancement with Ag–CuO/water hybrid nanofluid. *Results Phys.* **2017**, *7*, 2317–2324. [CrossRef]
4. Zainal, N.A.; Nazar, R.; Naganthran, K.; Pop, I. Unsteady stagnation point flow of hybrid nanofluid past a convectively heated stretching/shrinking sheet with velocity slip. *Mathematics* **2020**, *8*, 1649. [CrossRef]
5. Daniel, Y.S.; Aziz, Z.A.; Ismail, Z.; Salah, F. Double stratification effects on unsteady electrical MHD mixed convection flow of nanofluid with viscous dissipation and Joule heating. *J. Appl. Res. Technol.* **2017**, *15*, 464–476. [CrossRef]
6. Xie, H.; Jiang, B.; Liu, B.; Wang, Q.; Xu, J.; Pan, F. An investigation on the tribological performances of the SiO_2/MoS_2 hybrid nanofluids for magnesium alloy-steel contacts. *Nanoscale Res. Lett.* **2016**, *11*, 1–17. [CrossRef]
7. Afrand, M.; Toghraie, D.; Ruhani, B. Effects of temperature and nanoparticles concentration on rheological behavior of Fe3O4–Ag/EG hybrid nanofluid: An experimental study. *Exp. Therm. Fluid Sci.* **2016**, *77*, 38–44. [CrossRef]
8. Ghadikolaei, S.; Yassari, M.; Sadeghi, H.; Hosseinzadeh, K.; Ganji, D. Investigation on thermophysical properties of TiO_2–Cu/H_2O hybrid nanofluid transport dependent on shape factor in MHD stagnation point flow. *Powder Technol.* **2017**, *322*, 428–438. [CrossRef]

9. Hussain, S.; Ahmed, S.E.; Akbar, T. Entropy generation analysis in MHD mixed convection of hybrid nanofluid in an open cavity with a horizontal channel containing an adiabatic obstacle. *Int. J. Heat Mass Transf.* **2017**, *114*, 1054–1066. [CrossRef]
10. Waqas, M.; Farooq, M.; Khan, M.I.; Alsaedi, A.; Hayat, T.; Yasmeen, T. Magnetohydrodynamic (MHD) mixed convection flow of micropolar liquid due to nonlinear stretched sheet with convective condition. *Int. J. Heat Mass Transf.* **2016**, *102*, 766–772. [CrossRef]
11. Zhao, G.; Jian, Y.; Li, F. Streaming potential and heat transfer of nanofluids in microchannels in the presence of magnetic field. *J. Magn. Magn. Mater.* **2016**, *407*, 75–82. [CrossRef]
12. Yadav, D.; Wang, J.; Bhargava, R.; Lee, J.; Cho, H.H. Numerical investigation of the effect of magnetic field on the onset of nanofluid convection. *Appl. Therm. Eng.* **2016**, *103*, 1441–1449. [CrossRef]
13. Chamkha, A.; Rashad, E.; El-Zahar, H.A.; EL-Mky, H.A. Analytical and numerical investigation of Fe_3O_4–water nanofluid flow over a moveable plane in a parallel stream with high suction. *Energies* **2019**, *12*, 198. [CrossRef]
14. El-Kabeir, S.M.M.; El-Zahar, E.R.; Modather, M.; Gorla, R.S.R.; Rashad, A.M. Unsteady MHD slip flow of a ferrofluid over an impulsively stretched vertical surface. *AIP Adv.* **2019**, *9*, 045112. [CrossRef]
15. Crane, L.J. Flow past a stretching plate. *Z. Angew. Math. Phys.* **1970**, *21*, 645–647. [CrossRef]
16. Sandeep, N.; Sulochana, C.; Kumar, B.R. Unsteady MHD radiative flow and heat transfer of a dusty nanofluid over an exponentially stretching surface. *Eng. Sci. Technol. Int. J.* **2016**, *19*, 227–240. [CrossRef]
17. Nayak, M.; Akbar, N.S.; Tripathi, D.; Khan, Z.; Pandey, V. MHD 3D free convective flow of nanofluid over an exponentially stretching sheet with chemical reaction. *Adv. Powder Technol.* **2017**, *28*, 2159–2166. [CrossRef]
18. Hayat, T.; Nadeem, S. Flow of 3D Eyring-Powell fluid by utilizing Cattaneo-Christov heat flux model and chemical processes over an exponentially stretching surface. *Results Phys.* **2018**, *8*, 397–403. [CrossRef]
19. Rehman, F.U.; Nadeem, S.; Haq, R.U. Heat transfer analysis for three-dimensional stagnation-point flow over an exponentially stretching surface. *Chin. J. Phys.* **2017**, *55*, 1552–1560. [CrossRef]
20. Magyari, E.; Keller, B. Heat and mass transfer in the boundary layers on an exponentially stretching continuous surface. *J. Phys. D Appl. Phys.* **1999**, *32*, 577. [CrossRef]
21. Mushtaq, M.A.; Farooq, R.; Sharif, M.; Razzaq, M. The impact of variable fluid properties on hydromagnetic boundary layer and heat transfer flows over an exponentially stretching sheet. *J. Phys. Commun.* **2019**, *3*, 095005. [CrossRef]
22. Ferdows, M.; Khan, M.; Alam, M.; Sun, S. MHD mixed convective boundary layer flow of a nanofluid through a porous medium due to an exponentially stretching sheet. *Math. Probl. Eng.* **2012**, *2012*, 408528. [CrossRef]
23. Rahman, A.N.H.; Bachok, N.; Rosali, H. *Numerical Solutions of Mhd Stagnation-Point Flow over an Exponentially Stretching/Shrinking Sheet in a Nanofluid*; Journal of Physics: Conference Series; IOP Publishing: Philadelphia, PA, USA, 2019; p. 012012.
24. Hiemenz, K. Die Grenzschicht an einem in den gleichformigen Flussigkeitsstrom eingetauchten geraden Kreiszylinder. *Dinglers Polytech. J.* **1911**, *326*, 321–324, 344–348, 357–362, 372–376, 391–393, 407–410.
25. Homann, F. Der Einfluβ groβer Zähigkeit bei der Strömung um den Zylinder und um die Kugel. *Z. Angew. Math. Mech.* **1936**, *16*, 153–164. [CrossRef]
26. Wang, C. Stagnation flow towards a shrinking sheet. *Int. J. Non-Linear Mech.* **2008**, *43*, 377–382. [CrossRef]
27. Yacob, N.A.; Ishak, A.; Pop, I. Melting heat transfer in boundary layer stagnation-point flow towards a stretching/shrinking sheet in a micropolar fluid. *Comput. Fluids* **2011**, *47*, 16–21. [CrossRef]
28. Liao, S. On the homotopy analysis method for nonlinear problems. *Appl. Math. Comput.* **2004**, *147*, 499–513. [CrossRef]
29. Nasir, S.; Shah, Z.; Islam, S.; Bonyah, E.; Gul, T. Darcy Forchheimer nanofluid thin film flow of SWCNTs and heat transfer analysis over an unsteady stretching sheet. *AIP Adv.* **2019**, *9*, 015223. [CrossRef]
30. Tlili, W.; Khan, I.; Khan, I. Multiple slips effects on MHD SA-Al2O3 and SA-Cu non-Newtonian nanofluids flow over a stretching cylinder in porous medium with radiation and chemical reaction. *Results Phys.* **2018**, *8*, 213–222. [CrossRef]
31. Khan, N.S.; Shah, Z.; Islam, S.; Khan, I.; Alkanhal, T.A.; Tlili, I. Entropy generation in MHD mixed convection non-Newtonian second-grade nanoliquid thin film flow through a porous medium with chemical reaction and stratification. *Entropy* **2019**, *21*, 139. [CrossRef]
32. Fiza, M.; Islam, S.; Ullah, H.; Shah, Z.; Chohan, F. An asymptotic method with applications to nonlinear coupled partial differential equations. *Punjab Univ. J. Math.* **2018**, *50*, 139–151.
33. Abbas, I.A.; Abo-Dahab, S. On the numerical solution of thermal shock problem for generalized magneto-thermoelasticity for an infinitely long annular cylinder with variable thermal conductivity. *J. Comput. Theor. Nanosci.* **2014**, *11*, 607–618. [CrossRef]
34. Li, C.; Guo, H.; He, T.; Tian, X. Thermally nonlinear non-Fourier piezoelectric thermoelasticity problems with temperature-dependent elastic constants and thermal conductivity and nonlinear finite element analysis. *Waves Random Complex Media* **2022**, 1–38. [CrossRef]
35. Mohamed, R.; Abbas, I.A.; Abo-Dahab, S. Finite element analysis of hydromagnetic flow and heat transfer of a heat generation fluid over a surface embedded in a non-Darcian porous medium in the presence of chemical reaction. *Commun. Nonlinear Sci. Numer. Simul.* **2009**, *14*, 1385–1395. [CrossRef]
36. Rahbar, H.; Javanbakht, M.; Ziaei-Rad, S.; Reali, A.; Jafarzadeh, H. Finite element analysis of coupled phase-field and thermoelasticity equations at large strains for martensitic phase transformations based on implicit and explicit time discretization schemes. *Mech. Adv. Mater. Struct.* **2022**, *29*, 2531–2547. [CrossRef]